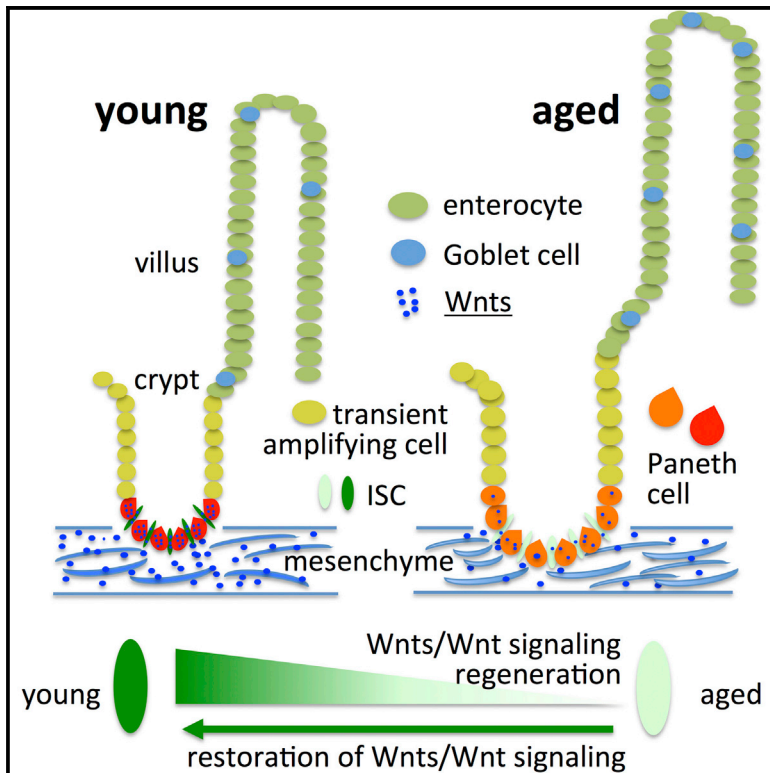# Canonical Wnt Signaling Ameliorates Aging of Intestinal Stem Cells

Graphical Abstract

Authors

Kodandaramireddy Nalapareddy,
Kalpana J. Nattamai, Rupali S. Kumar, ...,
Michael A. Helmrath, Yi Zheng,
Hartmut Geiger

Correspondence

hartmut.geiger@cchmc.org

In Brief

Nalapareddy et al. find that the decline of canonical Wnt signaling in intestinal stem cells (ISCs) leads to decreased ISC regenerative potential upon aging. Addition of exogenous Wnts in vitro improves regeneration of aged ISCs.

Highlights

- Aging alters intestinal architecture and intestinal stem cell (ISC) function

- ISC function is altered because of reduced canonical Wnt signaling upon aging

- Canonical Wnts are reduced in ISCs, Paneth cells, and mesenchyme

- Reactivating canonical Wnt signaling in aged ISCs restores function in organoids

Accession Numbers

GSE84061

CrossMark

CellPress

Canonical Wnt Signaling Ameliorates Aging of Intestinal Stem Cells

Kodandaramireddy Nalapareddy,[1] Kalpana J. Nattamai,[1] Rupali S. Kumar,[1] Rebekah Karns,[6]
Kathryn A. Wikenheiser-Brokamp,[3] Leesa L. Sampson,[1] Maxime M. Mahe,[4] Nambirajan Sundaram,[4]
Mary-Beth Yacyshyn,[5] Bruce Yacyshyn,[5] Michael A. Helmrath,[4] Yi Zheng,[1] and Hartmut Geiger[1,2,7,*]

[1]Division of Experimental Hematology and Cancer Biology, Cincinnati Children's Hospital Medical Center and University of Cincinnati, Cincinnati, OH 45229, USA
[2]Institute for Molecular Medicine, Stem Cells, and Aging and Aging Research Center, Ulm University, 89081 Ulm, Germany
[3]Divisions of Pathology and Laboratory Medicine and Pulmonary Biology, Perinatal Institute, Cincinnati Children's Hospital Medical Center and Department of Pathology and Laboratory Medicine, University of Cincinnati, Cincinnati, OH 45229, USA
[4]Division of Pediatric General and Thoracic Surgery, Cincinnati Children's Hospital Medical Center and University of Cincinnati, Cincinnati, OH 45229, USA
[5]Division of Digestive Diseases, University of Cincinnati, Cincinnati, OH 45229, USA
[6]Division of Gastroenterology, Hepatology, and Nutrition, Cincinnati Children's Hospital Medical Center and University of Cincinnati, Cincinnati, OH 45229, USA
[7]Lead Contact
*Correspondence: hartmut.geiger@cchmc.org
http://dx.doi.org/10.1016/j.celrep.2017.02.056

SUMMARY

Although intestinal homeostasis is maintained by intestinal stem cells (ISCs), regeneration is impaired upon aging. Here, we first uncover changes in intestinal architecture, cell number, and cell composition upon aging. Second, we identify a decline in the regenerative capacity of ISCs upon aging because of a decline in canonical Wnt signaling in ISCs. Changes in expression of Wnts are found in stem cells themselves and in their niche, including Paneth cells and mesenchyme. Third, reactivating canonical Wnt signaling enhances the function of both murine and human ISCs and, thus, ameliorates aging-associated phenotypes of ISCs in an organoid assay. Our data demonstrate a role for impaired Wnt signaling in physiological aging of ISCs and further identify potential therapeutic avenues to improve ISC regenerative potential upon aging.

INTRODUCTION

Aging is a complex process, ultimately leading to a decline in tissue regenerative capacity and organ maintenance. A decline in stem cell function upon aging might be one underlying factor for aging-associated changes in stem cell-driven tissues (Florian et al., 2013; Rando, 2006). The intestine is a stem cell-based organ. Already in the late 1990s, Martin et al. (1998a, 1998b) reported a functional decline in the regenerative potential of aged mouse small intestine during physiological aging and in response to irradiation. These studies reported delayed proliferation and increased apoptosis in aged small intestinal crypts (Martin et al., 1998a, 1998b). However, at that time, a lack of

markers for stem cells within the intestinal epithelium prevented more detailed analyses of the role of stem cell aging in aging-associated changes in the intestine. New marker systems now allow the prospective identification, purification, and analysis of intestinal stem cells (ISCs) upon aging. ISCs are located adjacent to differentiated Paneth cells at the base of cup-shaped invaginations called crypts. Above the crypt base is a highly proliferative transient amplifying zone that leads to protrusions called villi, which are primarily composed of enterocytes with intermingled secretary goblet cells and enteroendocrine cells (Barker et al., 2008). Evidence exists for a decline in regenerative function of intestinal epithelium upon DNA damage induced by short telomeres and reactive oxygen species (ROSs) (Jurk et al., 2014; Nalapareddy et al., 2010). However, the extent to which ISC function alters during physiological aging is still a matter of debate. Wnt signaling in the intestinal epithelium is well studied and critical for tissue homeostasis in young mice (Pinto et al., 2003; van der Flier et al., 2009b). Whether changes in Wnt signaling pathways contribute to changes in ISC function upon aging has so far not been determined. In this study, we show that aging results in a decline in ISC function and impaired regenerative capacity of the intestinal epithelium. Aged ISCs present with a decline in canonical Wnt signaling in ISCs and canonical Wnts themselves in both ISCs and stroma. This decline in canonical Wnt signaling is causative for the decline of ISC function, and further reactivation of canonical Wnt signaling ameliorates the impaired function of aged ISC, demonstrating that ISC aging is reversible.

RESULTS

Aging Alters Small Intestinal Crypt and Villus Architecture and Crypt Cell Proliferation

We first investigated changes in small intestinal architecture and histology upon aging, including crypt number, crypt size, and

villus length. Histological H&E analysis of intestinal tissue from young (2–3 months old) and aged mice (20–22 months old) showed a decrease in crypt number accompanied by an increase in crypt length and width in aged compared to young intestine in both the proximal and distal regions (Figures 1A–1H). Interestingly, the length of villi and the number of cells per crypt were also elevated in aged mice (Figures S1A–S1D). Aging thus results in changes in the architecture of the small intestine.

We next evaluated the extent of differences in cell proliferation in young and aged intestinal crypts and ISCs. Changes in proliferative potential have been, for example, associated with aging in muscle and hematopoietic compartments (Nalapareddy et al., 2010; Rando, 2006). Analyses of the mitotic index by phospho-histone H3 staining, which marks cells undergoing mitosis, revealed a decline in the number of mitotic cells in aged compared to young crypts (Figures 1I and 1J). To get additional insight into proliferative status upon aging, we performed bromodeoxyuridine (BrdU) tracing experiment. It takes approximately 4–5 days for a progenitor cell derived from an ISC division at the crypt base to reach the tip of the villus (Barker et al., 2008). The distance of migration is determined by the speed of cell migration and the proliferation status of the ISC as newly emerging crypt cells, upon ISC division, push older cells toward the tip of the villus. Our data revealed that the average distance of BrdU-positive cells that had traveled from the crypt base into the villi 72 hr post BrdU administration was larger in young mice compared to aged mice (Figures 1K and 1L), consistent with fewer mitotic events of ISCs and/or reduced transit-amplifying cell proliferation rates upon aging. We further investigated changes in the expression of cell cycle regulators and the level of apoptosis upon aging, both of which might be linked to the decline in the number of mitotic crypts. Consistent with a reduced rate in mitotic progression, expression of *CDKN1C* (p57) was reduced in aged intestinal crypts, whereas other cell cycle regulators like *CDKN1A* (p21), *CDKN1B* (p27), and *CDKN2A* (p16), and *Cyclin D1* showed no significant change upon aging (Figure S1E) (all FAM labeled real-time PCR primers are listed in Table 1). We also observed an increase in terminal deoxynucleotidyl transferase dUTP nick end labeling (TUNEL)-positive (apoptotic) cells in aged mouse intestinal crypts (Figures S1F and S1G). Taken together, these results indicate that aging alters the crypt and villus architecture and that aged crypts exhibit reduced cell divisions and reduced survival.

Aging Affects ISC Markers and Canonical Wnt Signaling

To investigate whether there are changes in ISC number upon aging, we analyzed intestinal tissue from young and aged *Lgr5-eGFP-IRES-CreER^T2* reporter mice (Barker et al., 2007), as *Lgr5* is an established marker of ISCs (Barker et al., 2007). Interestingly, we did not observe a significant change in the number of crypts positive for *Lgr5*-EGFP (Figures 2A and 2B) as well as in the percentage of Lgr5 EGFPhi cells (as determined by flow cytometric analyses) (Figure S2A) as well as for the total number of Lgr5EGFPhi ISCs (Figure 2C) at the crypt base at positions 0 to +4 (Barker et al., 2007) in aged compared to young animals. On the other hand, our observation of no changes in ISC numbers upon aging is consistent with a previous report investi-

gating aging-associated changes in crypts based on continuous clonal labeling approaches (Kozar et al., 2013). Because of the mosaic nature of the Lgr5-EGFP marker, which might hamper detailed quantitative analyses, we used another well-established ISC marker, Olfm4 (van der Flier et al., 2009a), to study ISCs upon aging. In situ hybridization experiments indicated that *Olfm4* cells are present at the crypt base in both young and aged intestinal crypts. *Olfm4* RNA expression levels were also similar in young and aged intestinal crypts (Figures 2D and 2E). In addition, we determined the expression levels of other markers more recently assigned to be specific for ISCs in crypts. Expression analyses of published *+4* quiescent ISC markers (*Lrig1*, *Hopx*, *Sox9*, *Tert*, and *Bmi1*) revealed that the expression of *Lrig1* and *Tert* were reduced (Figure 2F), whereas the expression levels of *Hopx*, *Sox9*, and *Bmi1* (Figure 2F) did not change upon aging. *Lrig1* controls ISC proliferation (Wong et al., 2012), and *Tert* is involved in the maintenance of stemness of stem cells in the intestine and other stem cell compartments (Montgomery et al., 2011; Nalapareddy et al., 2008). Together, these data imply that aging does not result in a change in the absolute number of ISCs, though some intestinal stem cell markers (Lrig1 and Tert) present with a decrease in expression. To initially evaluate the extent of changes in ISC function upon aging, we performed short-term lineage tracing experiment on young (2–3 months old) and aged (22–24 months old) *Lgr5-eGFP-IRES-CreER^T2*: *Rosa26^YFP* mice (Figures 1K and 1L). One week after yellow fluorescent protein (YFP) activation, Lgr5 EGFP-positive cells from crypts of young animals presented with YFP tracing into the villus, whereas the YFP-marked villus was subtle in aged mice (Figures S2B–S2D). Analyses 4 weeks after YFP activation in ISCs showed similar results compared to that of the 1-week time point (Figures 2G and 2H), indicating impaired ISC function upon aging. Similar results were obtained with 3 days of YFP activation followed by analysis 1 week after YFP activation (Figures S2E–S2G). In aggregation, these data imply that, rather than the number, the function of ISCs might be altered upon aging.

To delineate the molecular mechanisms of aging associated with ISCs or niche cells (Paneth cells), RNA sequencing (RNA-seq) analyses were performed on isolated Lgr5 EGFPhi-positive ISCs (Figure S3A) and CD24 hi-positive Paneth cells (Figure S3B; Kim et al., 2014; Sato et al., 2011) RNA-seq analysis revealed changes in the gene expression profile in both Lgr5 intestinal stem cells as well as in CD24 hi Paneth cells (Figures S3C and S3D). Molecular processes identified by Gene Ontology (GO) terminology that were downregulated in aged ISCs included, as anticipated, cell proliferation but also extracellular matrix, PPAR and SMAD signaling, and Wnt signaling pathways (Figure 3A; Figure S4A). We subsequently focused on changes in Wnt signaling upon aging because of its prominent role in the regulation of young ISCs.

As expected and known from young animals (Farin et al., 2012), the level of expression of Wnt ligands was higher in Paneth cells irrespective of their age, whereas the expression of Wnt target genes was higher in ISCs compared to Paneth cells irrespective of their age (Figure 3B). Quantitative real-time RT-PCR analyses for expression of *Wnt1*, *2*, *2b*, *3*, *3a*, *8a*, *8b*, *10a*, and *10b* (Farin et al., 2012) in ISCs demonstrated reduced *Wnt3* (Figure 3C) levels in aged ISCs. Paneth (niche) cells also
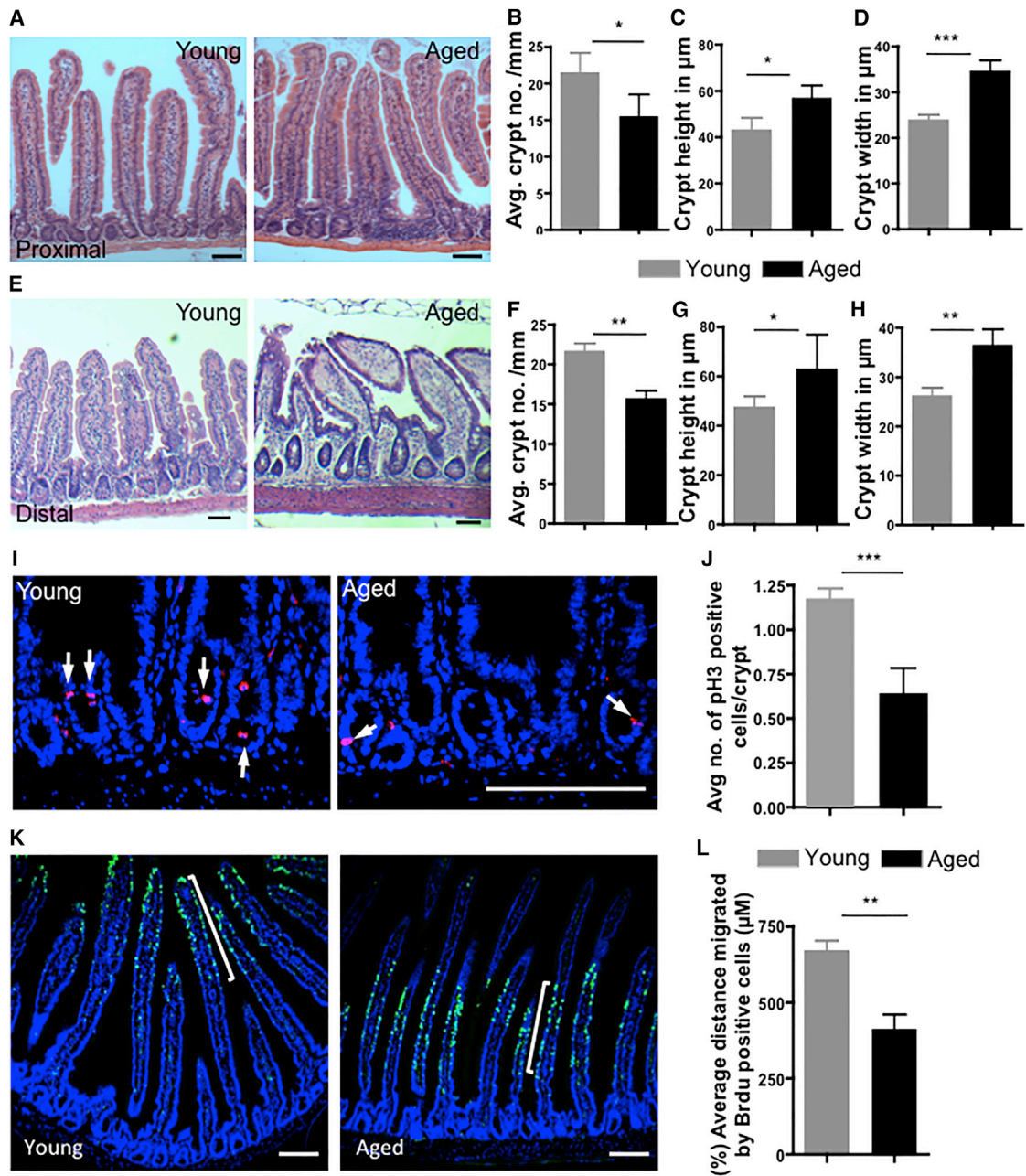
Figure 1. Aging Alters the Architecture of the Intestinal Crypt and Villus and Proliferation

(A) Representative picture of H&E-stained longitudinal sections of the proximal part of the intestine (duodenum) from 2- to 3-months-old (young) and 20- to 22-month-old (aged) mice. Scale bars, 100 μm.

(B) Number of crypts per millimeter of small intestine of young and aged mice.

(C and D) Average height (C) and width (D) of the crypts in duodenum from young and aged mice.

(E) Representative picture of H&E-stained longitudinal sections of the distal part of the intestine (ileum) from young and aged mice. Scale bars, 100 μm.

(F) Number of crypts per millimeter of the distal part (ileum) of small intestine of young and aged mice.

(G and H) Average height (G) and width (H) of the crypts in ileum.

(I) Representative pictures of anti-phospho-histone 3 (pH3) staining in young and aged intestinal crypts. Scale bar, 100 μm.

(J) Number of pH3-positive cells per crypt in young and aged intestine.

(K) Representative pictures of BrdU-stained young and aged mouse small intestine 72 hr after BrdU treatment. Scale bars, 100 μm.

(L) Distance from the crypt base to the middle of the BrdU-positive stripe in the proximal part of young and aged mouse small intestine 72 hr after BrdU treatment.

n = 3–4 mice/experimental group. *$p < 0.05$, **$p < 0.01$, ***$p < 0.001$. Error bars indicate SD.

Table 1. FAM-Labeled Real-Time PCR Primers for Mouse from ABI

Actin	Mm00607939_s1
Axin2	Mm00443610_m1
Ascl2	Mm01268891_g1
Lgr5	Mm00438890_m1
Ctnnb1	Mm00483039_m1
mTert	Mm00436931_m1
Olfm4	Mm01320260_m1
Bmi1	Mm03053308_g1
Hopx	Mm00558630_m1
Lrig1	Mm00456116_m1
Sox9	Mm00448840_m1
Ccnd1	Mm00432359_m1
Notch1	Mm00435249_m1
Notch2	Mm00803077_m1
Notch3	Mm01345646_m1
Notch4	Mm00440525_m1
p16 (Cdkn2a)	Mm00494449_m1
p27 (Cdkn1b)	Mm00438168_m1
p57 (Cdkn1c)	Mm01272135_g1
p21 (Cdkn1a)	Mm04205640_g1
Atoh1	Mm00476035_s1
Wnt3	Mm00437336_m1
Wnt2	Mm00470018_m1
Ephb2	Mm01181021_m1
Myc	Mm00487804_m1
Cd44	Mm01277161_m1

presented with reduced Wnt3 expression levels (Figure 3D). However, expression of other Wnts (like *Wnt1*, *2*, *3a*, *8a*, *8b*, *10a*, and *10b*) in both ISCs and Paneth cells was below our threshold level (data not shown). Mesenchyme has been recently been identified as an ISC niche and support system for ISCs (Farin et al., 2012; Smith et al., 2012). Quantitative analyses on expression of canonical Wnts in mesenchyme (in the absence of crypt epithelium) from young and aged mouse small intestine also revealed a decline in *Wnt3* but, for example, not for *Wnt2b* and *Wnt2* (Figures 3E and 3F; Figure S4B), whereas the other Wnts tested were, again, below our threshold level of detection (data not shown). Finally, canonical Wnt signaling target genes and genes regulating ISC function, like *β-catenin*, *Ascl2*, *Lgr5*, *Myc*, *Ephb2*, and *CD44* (van der Flier et al., 2009b) presented with a decline in the level of expression in ISCs but, interestingly, not *CyclinD1*, *Axin2*, or *Olfm4* (Figure 3G). Similar data were obtained when young and aged crypts were analyzed for levels of gene expression, like a reduction in the expression of *Wnt3*, *β-catenin*, *Ascl2*, and *Lgr5*, upon aging, except for *Axin2*, which was also down in whole-crypt analysis. (Figures S4C and S4D). At the protein level, *Ascl2* and nuclear β catenin were reduced (Figures S4E and S4F) in aged intestinal crypts.

Together, these data imply a decline of canonical Wnt signaling in ISCs upon aging, which is linked to a decline in expression of canonical Wnts like Wnt3 in both Paneth cells

and the mesenchyme as well as in ISCs themselves. Notch signaling, together with Wnt signaling, regulates ISC differentiation (Tian et al., 2015). We also observed a decline in the expression of *Notch1* (Figure 3H) (expression of *Notch2*, *3*, and *4* was not detected in ISCs; data not shown) and an increase in Atonal homolog 1 (*Atoh1*) (Figure 3I) gene expression. Atoh1 is a secretory-specific transcription factor described to control lateral inhibition through delta-like notch ligand genes in young crypts and also to drive the expression of numerous secretory lineage genes (Kim et al., 2014). Therefore, these data also suggest altered ISC differentiation upon aging.

Aging Affects Differentiation in the Intestinal Compartment

The aging-associated changes in canonical Wnt and Notch signaling might result in changes in the differentiation potential of aged ISCs. We thus quantified the number of goblet and Paneth cells in the aged intestine. Goblet and Paneth cells stem from ISCs. The number of Paneth cells per crypt, as determined by lysozyme or MMP7 staining, in both the proximal and distal mouse intestine was increased upon aging (Figures 4A and 4B; Figures S4G and S4H). The number of goblet cells (determined by Alcian blue staining), a secretory cell type, was also increased in aged compared to young mouse intestine (Figures 4C and 4D). Our finding of an increase in the number of differentiated secretory cells upon aging is consistent with reduced Notch signaling along with an increase in the expression levels of Atoh1, which all favor ISC differentiation. Aging thus also results in an increase in the number of secretary lineage cells, including Paneth cells and goblet cells, most likely driven by changes in the differentiation potential of aged ISCs. This increase in Paneth cell number, though, does not compensate for the overall lower level of expression of Wnt3 upon aging because overall Wnt signaling is reduced in aged ISCs.

Aging Attenuates the Regenerative Capacity of ISCs

Aged muscle and hematopoietic stem cells present with reduced regenerative potential (Geiger et al., 2013; Rando, 2006; Rossi et al., 2008). Whether aging also results in a decline in ISC regenerative potential in vivo was addressed in assays determining the regenerative response to ionizing radiation. Irradiation in the intestinal epithelium is accompanied by crypt shrinking because of apoptosis, followed by a burst of proliferative response predominantly from existing/surviving ISCs (Metcalfe et al., 2014), usually leading to an increase in crypt depth followed by crypt fission. Analysis of the mouse small intestine 5 days after 10 Gy of irradiation (Figure 5A) showed a higher number of Ki67-negative, or non-proliferative, crypts (Figures 5B and 5C) in aged compared to young intestine. These findings can be explained by both an increase in apoptosis (Figures S5A and S5B) or a delayed regenerative response. To further delineate the extent of a change in regenerative function of ISCs upon aging, we employed two consecutive doses of 10-Gy irradiation 24 hr apart (Figure 5D; referred to as 10+10 Gy) to model additional serial stress and induction of regeneration (Geiger et al., 2013). We observed a strong decline 3 days after 10+10 Gy irradiation in the number of viable crypts in the young intestinal epithelium compared to the non-irradiated control (Figures S5C and S5D).
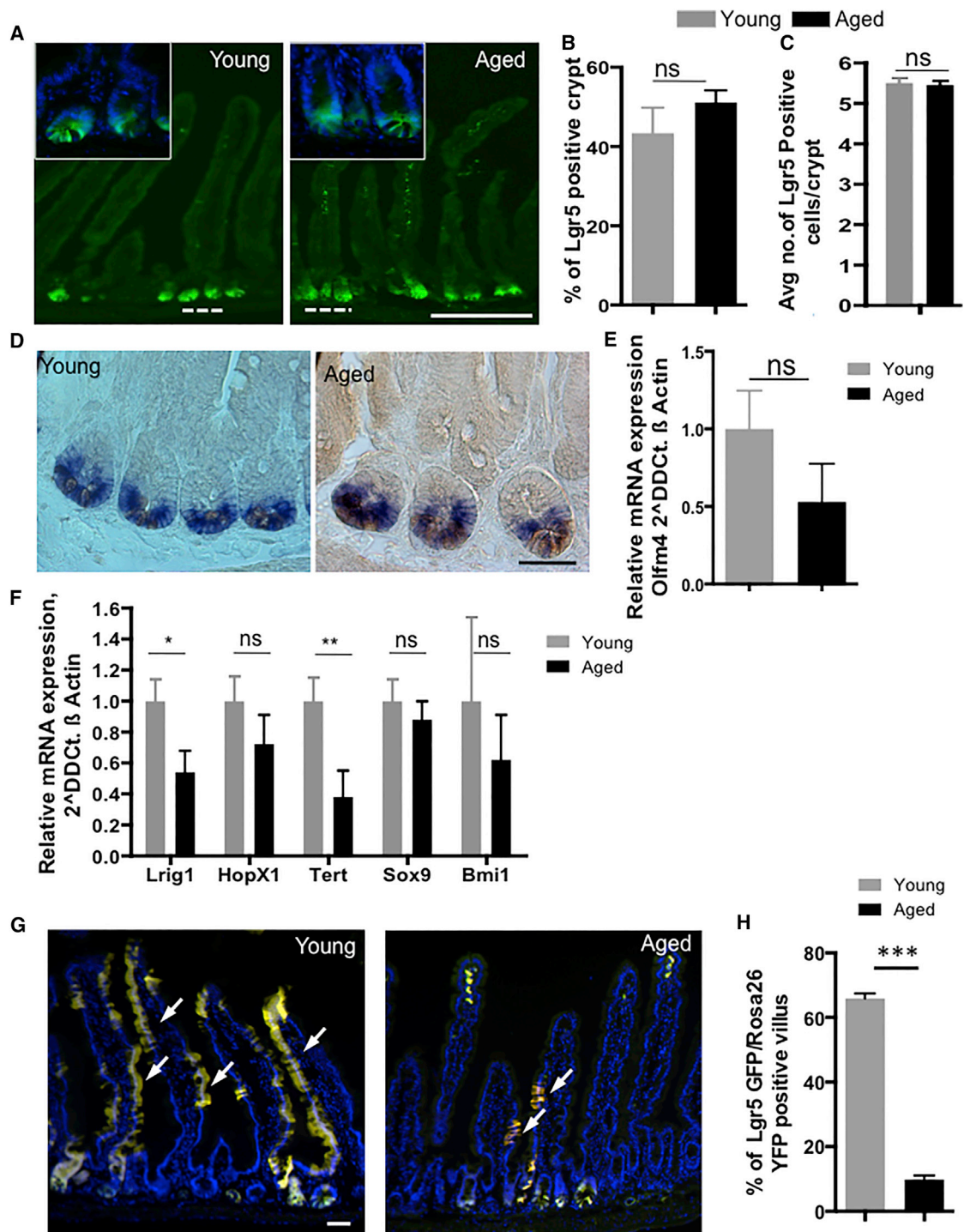
Figure 2. Effect of Aging on ISCs

(A) Representative picture of a formalin-fixed longitudinal cryosection of young and aged $Lgr5^{eGFPCreER(T2)}$ mice. Scale bar, 100 μm.

(B) Histogram showing the average percentage of Lgr5-positive (GFP-positive) crypts in the proximal part of young and aged mouse small intestine.

(C) Histogram showing the average number of Lgr5-positive (GFP-positive) cells from position 0 to +4 at the crypt base in the proximal part of young and aged mouse small intestine.

(D) Representative picture of Olfm4 in situ hybridization on young and aged mouse intestine. Scale bar, 50 μm. A blue/purple color indicates Olfm4 in situ staining, and a light brown color indicates lysozyme staining.

(E) *Olfm4* expression normalized to β *Actin* transcript levels in young and aged crypts of mouse small intestine.

(legend continued on next page)

We also detected a marked increase in crypt depth and crypt fission in young but not in aged intestines on day 5 after irradiation (Figures 5E–5H). In addition, ~50% of aged mice died by day 5 in response to 10+10 Gy compared to only 12% of young animals (data not shown). There was no difference in the number of viable crypts between young and aged mouse intestines on day 5 after irradiation (Figures S5C and S5D). These data support that young ISCs exhibit a greater regenerative potential compared with aged ISCs.

Restoring Canonical Wnt Signaling Ameliorates Aging of ISCs

To further investigate the extent of altered ISC regenerative potential upon aging, we determined the frequency of organoid formation of young and aged duodenal (proximal) crypts (Sato et al., 2009). The organoid system is an accepted ex vivo assay that is reflective of stem cell function in vivo (Boj et al., 2015). The ability to form organoids depends primarily on ISC function (Barker et al., 2007; Sato et al., 2009). Organoids derived from both young and aged intestinal epithelium were initially formed with equal efficiency (Figure S6A). Organoids from aged mice, though, had a reduced rate of organoid formation after the third passage (Figures 6A and 6B). In addition, the number of lobes or buds per crypt, another indicator of stem cell function, was lower in replated organoids from aged intestine (Figure 6C). Finally, organoids derived from crypts of young mice were able to form organoids through the termination of the assay at the eighth replating, whereas organoids from aged mice showed a severe decline in replating efficiency after the fourth split. These data demonstrate a decline in the regenerative potential of aged ISCs and are reminiscent of the loss of repopulating activity of aged haematopoietic stem cells (HSCs) upon serial transplantation (Kamminga et al., 2005).

If this decline in ISC function upon aging was a consequence of the decline in canonical Wnt signaling (Figures 3C and 3G), then restoration of canonical Wnt signaling in aged ISCs might improve their regenerative potential. Addition of Wnt3a, an inducer of canonical Wnt signaling, to aged organoid cultures resulted in an increase in the number of organoids and increase in the number of lobes/buds in organoids derived from aged animals compared to non-treated aged control organoids (Figures 6D–6F) almost to the level seen in cultures of young organoids. Addition of Wnt3a to aged organoid cultures resulted, as expected, in elevated levels of expression of the canonical Wnt target genes *Axin2* and *Ascl2* in aged organoids (Figure S6B). Re-activation of canonical Wnt signaling in aged crypts thus re-established a more youthful regenerative potential in aged ISCs. We finally investigated the extent of the aging-associated decline in human ISC function. Organoid cultures from young (12–16 years old) and aged (62–77 years old) human subjects showed, similar to the mouse, a decline in the frequency of orga-noid formation upon aging (Figures 6G and 6H) that was amelio-rated by addition of Wnt3a (Figures 6G and 6H). These data demonstrate an important role of reduced canonical Wnt signaling in aged ISCs in mice and humans that is tightly linked to reduced regenerative potential upon aging. Enhancing canon-ical Wnt signaling to a youthful level might thus be one approach to restore the function of aged ISCs to a more youthful level.

DISCUSSION

Stem cell aging is one underlying cause of aging in tissues that depend upon stem cell activity in the adult (Nalapareddy et al., 2008; Rando, 2006). The laboratory of Chris Potten pioneered the field of intestinal cell biology with the finding that aging impairs regeneration of mouse intestinal epithelium (Martin et al., 1998a; Potten et al., 1974). Our studies further substantiate but also significantly extend these findings by demonstrating that, upon aging, there is decreased ISC function and regenerative potential. Although the number of ISCs was not reduced upon aging, aged ISCs showed reduced regeneration upon serial radiation exposure (10+10 Gy) and a decline in organoid formation. Phospho-histone 3 staining demonstrates that the number of cells ultimately entering mitosis (mitotic index) is reduced in aged compared with young mouse intestinal crypt cells. This conclusion is further supported by BrdU tracing experiments in which BrdU-positive cells from young intestinal crypts travel farther into the villus compared with aged ones. Ultimately, ISC lineage tracing experiments with young and aged *Lgr5-EGFP-IRES-CreER^{T2}*: *Rosa26^{YFP}* animals further substantiate a decline in stem cell function and turnover upon aging. Previous reports (Kozar et al., 2013) indicated that the number of ISCs and the number of stem cells replaced are age-independent by using a specific labeling technique of intestinal epithelial cells at a young age with a follow-up to 2 years. This is distinct from our experiments of ISC-specific labeling and tracing at a distinct age (8–10 weeks and 22–24 months of age). However, further experiments are necessary to evaluate changes in intestinal clonality upon aging in more detail, comparing whole intestinal epithelial cell-specific, ISC-specific, and niche- (Paneth cell) and enterocyte-specific label-ing protocols.

The exclusive decline in p57 levels among a panoply of cell cycle regulators in the aged crypt is somewhat surprising, although low levels of p57 have been associated with stem cell hibernation (Yamazaki et al., 2006) and low levels of p57 upon aging were also detected in aged hematopoietic stem cells (Florian et al., 2012).

Besides a decline in Wnt signaling in aged ISCs, we also observed a decline in genes regulating extra cellular matrix proteins and genes that alter cell proliferation and changes in PPAR and SMAD signaling (Figure 3). Tissue damage upon aging

(F) *Lrig1*, *HopX1*, *Tert*, *Sox 9*, and *Bmi1* expression normalized to β actin transcript levels in young and aged crypts of mouse small intestine.
(G) Representative pictures of formalin-fixed longitudinal sections of the proximal part of young and aged *Lgr5^{eGFPCreER(T2)} Rosa26^{YFP}* mouse intestine 4 weeks after one shot of tamoxifen. Scale bar, 50 μm.
(H) Number of YFP-positive villus/Lgr5 EGFP-positive crypts in the proximal part of young and aged mouse intestine 4 weeks after one shot of tamoxifen.
All Expression data were analyzed with the 2^{-DDCt} method. All qRT-PCRs were performed on RNA isolated from crypts of the proximal part of mouse small intestine. n = 3–4 mice/experimental group. *p < 0.05, **p < 0.01, ***p < 0.001. Error bars represent SD.
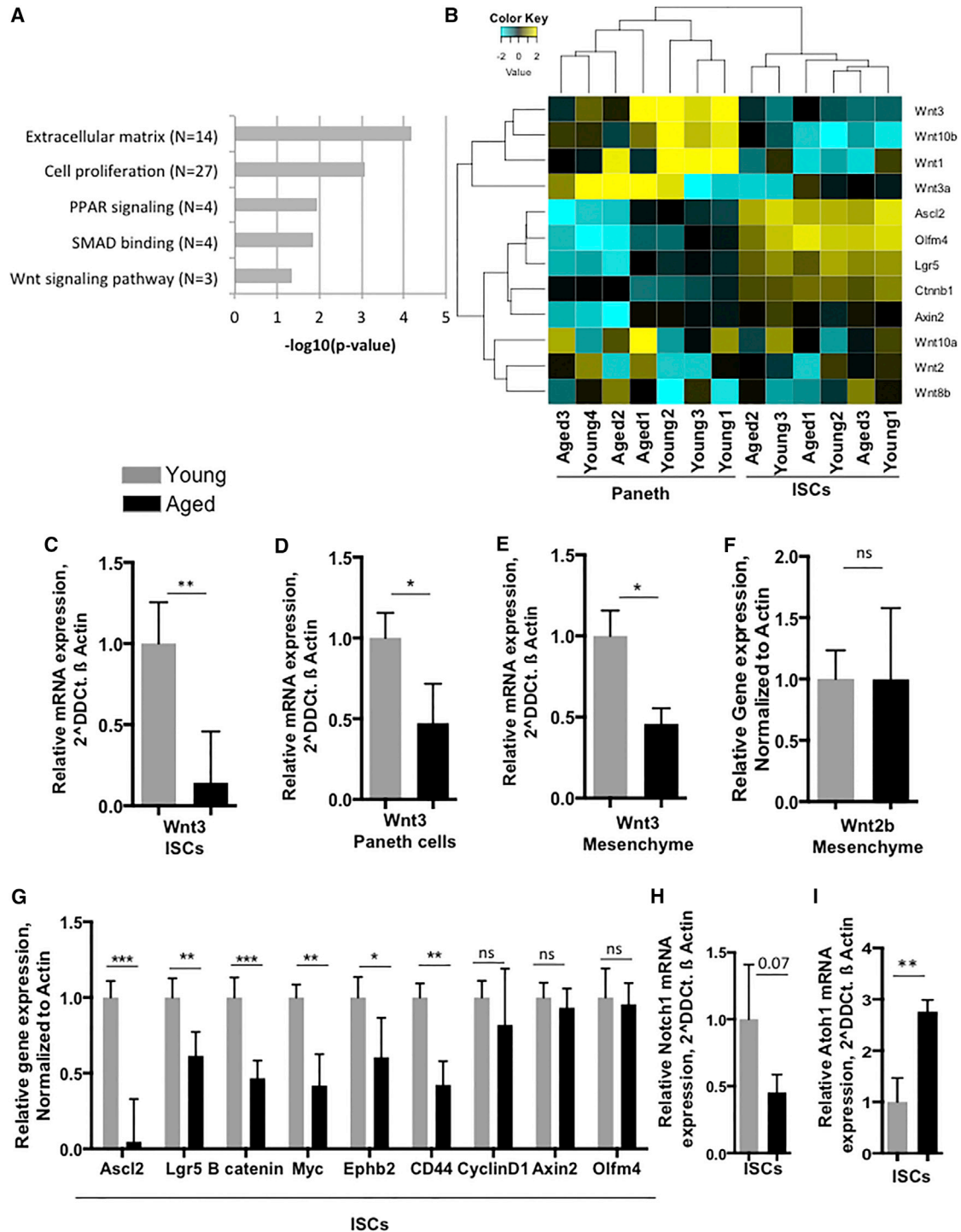
Figure 3. Aging Affects Gene Expression in ISCs and Niche

(A) Histogram showing the downregulated process in ISCs from aged intestine.

(B) Heatmap showing differential expression of Wnt genes in young and aged ISCs and Paneth cells.

(C) *Wnt3* expression normalized to *β Actin* transcript levels in young and aged ISCs of mouse small intestine.

(D) *Wnt3* expression normalized to *β Actin* transcript levels in young and aged Paneth cells.

(E) *Wnt3* expression normalized to *β Actin* transcript levels in young and aged mesenchyme of mouse small intestine.

(F) *Wnt2b* expression normalized to *β Actin* transcript levels in young and aged mesenchyme of mouse small intestine.
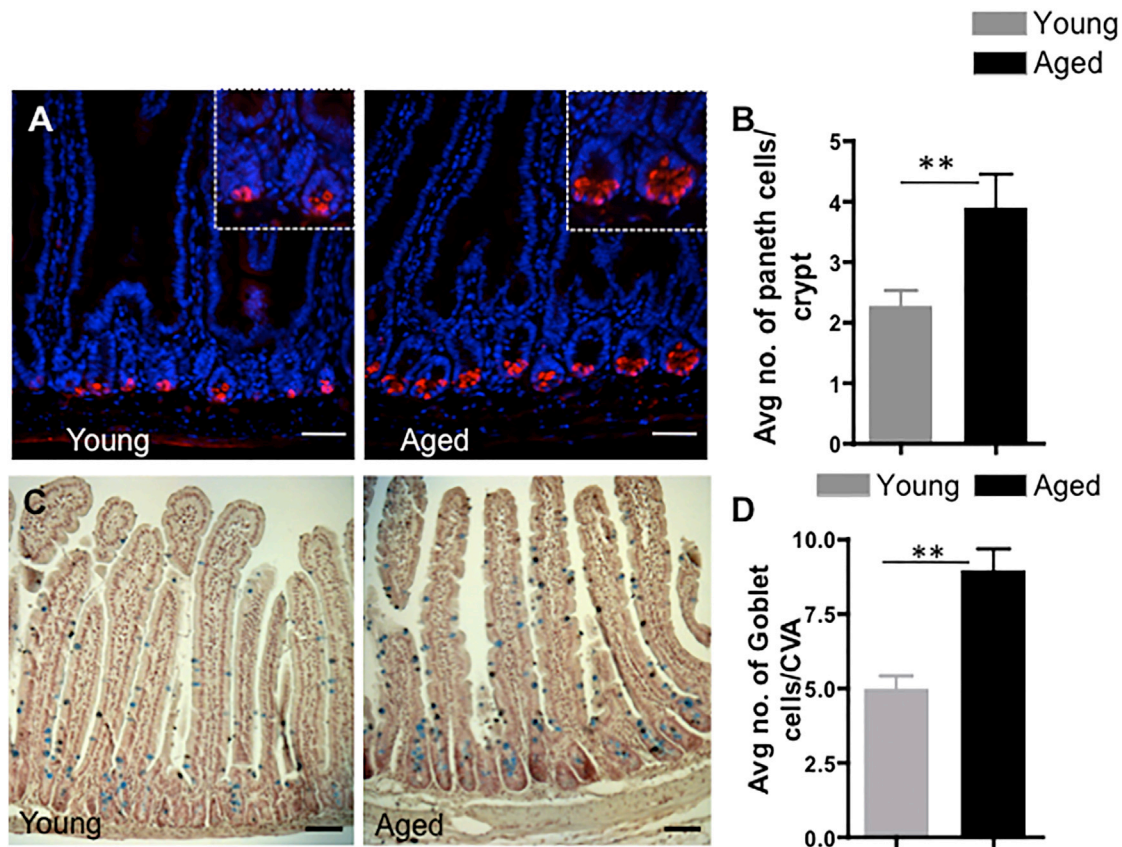
Figure 4. Aging Increases the Number of Intestinal Secretory Cells

(A) Representative picture of staining for lysozyme identifying Paneth cells (red) in the proximal part of young and aged mouse small intestine (nucleus, DAPI, blue). Scale bar, 50 μm.

(B) Number of lysozyme-positive cells per crypt in young and aged mice.

(C) Representative picture of Alcian blue staining identifying goblet cells in young and aged mice. Scale bar, 50 μm.

(D) Number of goblet cells per crypt villus axis in young and aged mice. Scale bar, 50 μm.

n = 3–4 mice/experimental group. *p < 0.05, **p < 0.01, ***p < 0.001. Error bars represent SD.

affects the extracellular matrix, which further alters stem cell niches regulating stem cell-regenerative functions (Blau et al., 2015), so changes in extracellular matrix proteins might further contribute to changes in the niche, which still has to be determined though. However, downregulation of cell proliferation genes could also be a consequence of Wnt signaling deregulation in ISCs (Figure 3G) and deregulation of genes affecting stem cell function, such as *Lrig1* (Figure 2F) and *Ephb2* (Figure 3G), in ISCs. Another possibility is that changes that affect cell adhesion and molecular changes affecting proliferation are actually directly linked. Whether Smad and PPAR signaling are linked to changes in Wnt signaling upon ISC aging or vice versa will also need further investigation.

Our data imply that primarily reduced canonical Wnt signaling in ISCs causes impaired ISC function upon aging.

We report here a decline in canonical Wnt signaling in ISCs and reduced canonical Wnt expression (primarily Wnt3) in both Paneth cells and mesenchyme, which might also contribute to the reduced activity of canonical Wnt/Wnt signaling in aged ISCs. Because it was recently reported that Wnt3 transfer requires direct cell contact and has only a very limited range (Farin et al., 2016), the most likely cellular source of Wnts that influence Wnt signaling upon aging might thus be mostly Paneth cells and, in part, mesenchyme. Our data also support a likely contribution of an ISC-intrinsic mechanism of changes in Wnt expression to reduced canonical signaling in ISCs upon aging. The precise molecular mechanisms that lead to reduced expression of canonical Wnts and Wnt signaling upon aging will require further investigation. It is interesting to note that *Ascl2*, and not primarily *Axin2*, seems to be

(G) *β Catenin*, *Axin 2*, *Ascl2*, and *Lgr5* expression normalized to *β Actin* transcript levels in young and aged ISCs.

(H and I) *Notch1* (H) and *Atoh1* (I) expression normalized to *β Actin* transcript levels in young and aged ISCs of mouse small intestine.

All qRT-PCRs were performed on RNA isolated from crypts of the proximal part of mouse small intestine. n = 3–5 mice/experimental group. *p < 0.05, **p < 0.01, ***p < 0.001. Error bars represent SD.
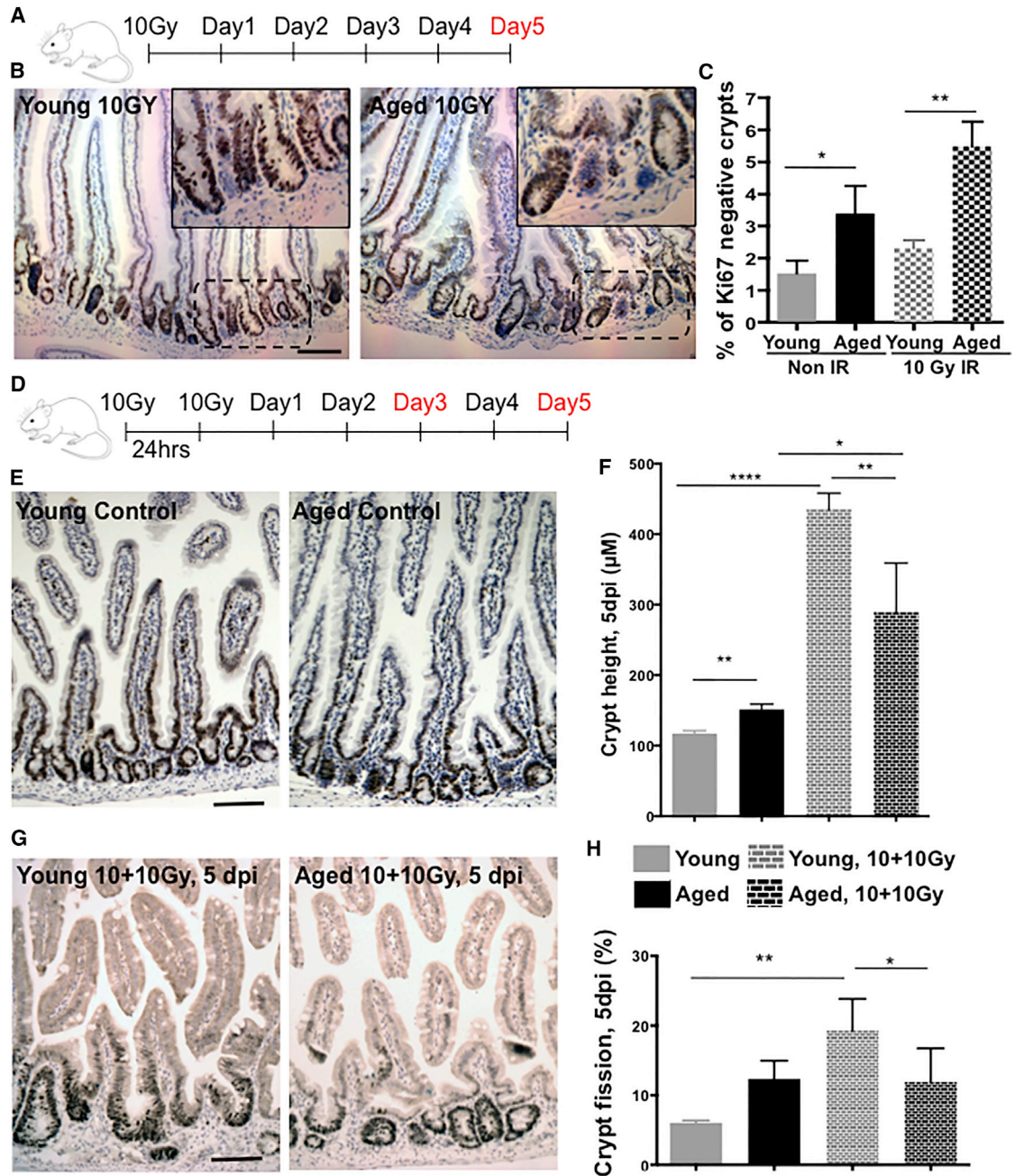
Figure 5. Impaired Regenerative Response in Aged Mouse Intestine

(A) Experimental setup.

(B) Representative picture of Ki67 staining in young and aged crypts 5 days after 10-Gy radiation. Scale bar, 100 μm.

(C) Percentage of Ki67-negative crypts in young and aged mice.

(D) Experimental setup.

(E) Representative picture of Ki67 staining in young and aged crypts without radiation (control). Scale bar, 100 μm.

(F) Crypt depth in the proximal part of mouse small intestine 5 days after 10+10-Gy radiation.

(G) Representative picture of Ki67 staining in young and aged crypts 5 days after 10+10-Gy radiation. Scale bar, 100 μm.

(H) Percentage of crypt fission in young and aged crypts 5 days after 10+10-Gy radiation.

n = 8 mice/experimental group. *$p < 0.05$, **$p < 0.01$, ***$p < 0.001$. Error bars represent SD.
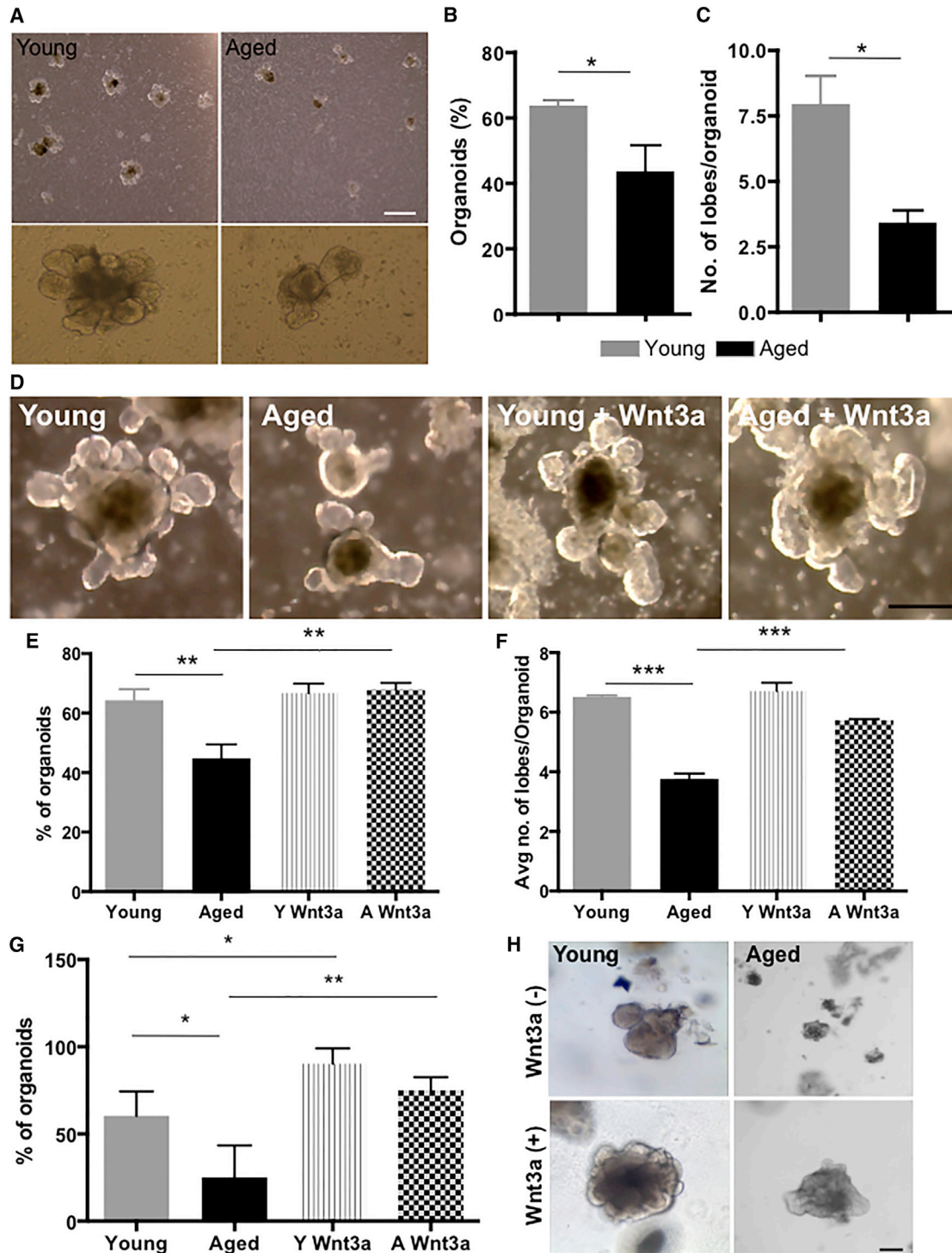
Figure 6. Restoration of Canonical Wnt Signaling in Aged Organoids Restores Youthful Function

(A) Representative picture of organoids of young and aged intestine after three passages as well as pictures of single organoids. Scale bar, 400 μm.

(B) Percentage of organoid growth after three passages.

(C) Number of lobes per organoid in organoids derived from young and aged crypts of mouse small intestine after three passages.

(D) Representative pictures of young and aged organoids in the presence or absence of recombinant Wnt3a. Scale bar, 100 μm.

(legend continued on next page)

the "aging" target gene of canonical Wnt signaling in ISCs because changes in the expression of *Ascl2* are closely correlated to the aging and rejuvenation phenotype reported here. Although *Axin2* is a strong prototype target gene of canonical Wnt signaling, as demonstrated in multiple publications, upon aging, in our study, Axin2 is not the gene linked to changes in Wnt Signaling in ISCs. Thus it is also a surprising finding that canonical changes in canonical Wnt signaling like *β catenin*, *Myc*, and *Ascl2* present with little or no correlation to *Axin2* expression. Our experiments reveal a critical role of a decline in *Ascl2* expression at both the RNA and protein levels upon aging in both crypts and ISCs. A contribution of changes in *Ascl2* expression to aging is consistent with a report demonstrating a central role for Ascl2 in determining ISC fate (van der Flier et al., 2009b). This finding is also in line with recent reports suggesting *Ascl2* as a central Wnt-responsive transcription factor (Schuijers et al., 2015). The increase in the number of secretory lineage cells, namely Paneth and goblet cells, also implies deregulation of stem cell differentiation pathways in aged ISCs, most likely as a response to deregulated Notch signaling, like elevated levels of Atoh1 expression (Kim et al., 2014; Koch et al., 2013; Tian et al., 2015). Additional studies are required to delineate the detailed interplay between Notch and Wnt signaling upon aging of ISCs.

Wnt signaling plays a prominent role in ISC maintenance in young animals (van der Flier et al., 2009b), and our data provide evidence that changes in Wnt signaling upon aging are causative for aging of intestinal ISCs because a youthful level of organoid formation can be achieved by re-activating canonical Wnt signaling in aged ISCs. Because mutations leading to hyperactivation of canonical Wnt signaling are linked to intestinal tumorigenesis (Gregorieff and Clevers, 2005), lowering Wnt signaling upon aging might be, among others, a mechanism to counter hyperactivation in the case of mutations in aged intestine, though at the expense of an overall reduced regenerative potential of ISCs. Our finding of a lower level of Wnt signaling upon ISC aging is distinct from reports of aging in the muscle stem cell compartment (Brack et al., 2007), in which elevated levels of Wnts were reported to cause aging of muscle stem cells. Our findings are in line with mechanisms of aging in the HSC compartment (Florian et al., 2013), in which aging of HSCs is also associated with low canonical Wnt signaling (Reya et al., 2003).

In summary, we demonstrate impaired ISC function in aged intestinal epithelium because of a decline in canonical Wnt signaling. Restoration of a more youthful phenotype of aged ISC function is achieved by reactivation of canonical Wnt signaling in both murine and human intestinal organoid cultures. These data suggest reactivation of canonical Wnt signaling to a youthful level as a potential therapeutic approach to restore youthfulness of ISC function to increase the regenerative capacity of aged intestinal epithelium.

EXPERIMENTAL PROCEDURES

Experimental Mice

Young (2–4 months old) male and female C57BL/6 mice were purchased from Charles River Laboratories and aged (18–22 months old) female C57BL/6 mice from NIA. *Lgr5*^{eGFPCreERT2} mice were purchased from Jackson Immuno-noResearch Laboratories (C57BL/6x129/SvEv mice). *Lgr5*^{eGFPCreERT2} mice were crossed with *Rosa26*^{YFP} mice to obtain *Lgr5*^{eGFPCreERT2} *Rosa26*^{YFP} mice (both male and female) and aged for up to 2 years. All analyses were performed on proximal (8–9 cm from the start of the small intestine) or distal part (the last 5–6 cm) of the small intestine. Animals were housed under specific pathogen-free conditions and handled in accordance with protocols approved by the Animal Care and Use Committee of Cincinnati Children's Hospital Medical Center.

Histology and Microscopy

Histological analysis was performed using H&E staining using standard histological protocols. Measurements for crypt depth and villus height were taken using ImageJ software on pictures taken from an Olympus CX41 microscope with Qcapture software. For goblet cell analysis, paraffin-embedded, 6-μm-thick samples were rehydrated and stained with Alcian blue solution (pH 2.6) and counterstained with nuclear fast red.

Irradiation Recovery Experiment

2- to 3-month-old young mice and 20- to 22-month-old aged mice were irradiated by the Cincinnati Children's Hospital Research Foundation (CCHRF) Comprehensive Mouse and Cancer core Facility using the model mark I-68A cesium 137 irradiator (JL Shepherd & Associates) with one dose of 10-Gy and harvested 5 days after irradiation or irradiated with 10 Gy followed by a second 10-Gy dose 24 hr later and harvested 3 days and 5 days after irradiation.

Immunohistochemistry and Immunofluorescence

Tissues were fixed overnight in 4% paraformaldehyde at 4°C and were washed three times in PBS. Fixed tissues were dehydrated and embedded in paraffin by the Cincinnati Children's Hospital Medical Center (CCHMC) Pathology core. Immunofluorescence was performed on 6-μm-thick paraffin sections. Sections were deparaffinized, rehydrated, and permeabilized in 10 mM sodium citrate buffer. Primary antibodies were incubated overnight at 4°C: Ki67 (Thermo Scientific, SP6, 1:100 dilution in PBS), lysozyme (Dako, 1:400 dilution in PBS), MMP7 (R&D Systems, 1:250 dilution in PBS), anti-BrdU antibody (Santa Cruz Biotechnology, 1:100 dilution in PBS), phospho-histone H3 (Cell Signaling Technology, 1:100 dilution in PBS). This was followed by washes with PBS and incubation with secondary antibodies: anti-mouse fluorescein isothiocyanate (FITC) (Jackson ImmunoResearch Laboratories, 1:200) and anti-rabbit Cy3 (Jackson ImmunoResearch Laboratories, 1:200) for 1 hr at room temperature. For cryo-embedding, fixed tissues were incubated overnight in 30% sucrose in PBS at 4°C and then embedded in optimal cutting temperature (OCT) compound (Sakura); sections were cut at 7-μm thickness. Tissues were permeabilized in 0.3% Triton X for 10 min and washed three times with PBS, and then we followed same protocol as mentioned above.

OLFM4 In Situ and Lysozyme Co-staining

6- to 9-μm-thick sections were deparaffinized, rehydrated, and treated with 0.2 M sodium chloride and proteinase K and fixed with 4% paraformaldehyde (PFA). Sections were prehybridized after being demethylated with acetic anhydride. Prehybridized sections were hybridized with 400 ng/ml Olfm4 probe labeled with digoxigenin (DIG) (Promega). Sections were incubated for 48–72 hr in a humid chamber at 62°C, washed, and incubated with secondary anti-DIG antibody (Roche) overnight at 4°C. Sections were washed and

---

(E and F) Percentage of organoid growth (E) and number of lobes per organoid (F) after three passages of young and aged organoids in the presence or absence of Wnt3a.

(G) Percentage of organoids derived from human small intestine at week 1 after initial plating in the presence or absence of recombinant Wnt3a.

(H) Representative pictures of organoids derived from young and aged human intestine. Scale bar, 100 μm.

Young, n = 4; aged, n = 5. *p < 0.05, **p < 0.01, ***p < 0.001. Error bars represent SD.

developed with nitro blue tetrazolium chloride/5-brom-4-chlor-3-indolyl phosphate for 2–4 hr. After washing, we incubated the sections with lysozyme antibody (Dako, 1:400 dilution in PBS) overnight at 4°C as mentioned above, followed by anti-rabbit secondary antibody and 3,3′-Diaminobenzidine (DAB) staining. Olfm4 in situ looks blue/purple, and lysozyme staining looks brown.

Crypt Isolation, Organoid Culture, ISC Isolation, and Gene Expression Analyses

Mouse small intestine was dissected and washed in cold PBS. Villi were removed by scraping with glass slides. Intestinal pieces were transferred to 5 mM EDTA in PBS (pH 8), followed by three 1-min shakings by hand with a 10-min incubation at 4°C. Intestinal pieces were removed and centrifuged at 800 rpm for 5 min, and then the pellet was resuspended in PBS followed by centrifugation at 600 rpm for 2 min. Isolated crypts were used for organoid culture or frozen at −80°C for further experiments. 500 or 1,000 crypts/well were mixed with Matrigel and plated in a 24-well plate, polymerized in an incubator at 37°C for 15 min, and overlaid with 500 μL of intestinal stem cell medium: DMEM/F12 (Invitrogen), 2 mM Gluta Max (Invitrogen), 10 mM 4-(2-hydroxyethyl)-1-piperazineethanesulfonic acid (HEPES) buffer (Sigma), 0.5 U/mL penicillin/streptomycin (Invitrogen), N2 and B27 supplement 1× (Invitrogen), 50 ng/mL mouse recombinant epithelial growth factor (Invitrogen), 100 ng/mL mouse recombinant Noggin (PeproTech), and 500 ng/mL human recombinant R-spondin1 (PeproTech). 100 ng/mL mouse recombinant Wnt3A (PeproTech) was added only to cultures for rescue experiments. For regular use, our intestinal stem cell medium did not contain Wnt3a. The medium was changed 2 days after initial plating. On the sixth day after initial plating, organoid numbers and number of lobes per organoid were counted. Organoids were passaged by taking out the medium and dissolving the Matrigel in ice-cold DMEM, and then the medium with the dissolved Matrigel was pipetted 25 times with a 200-μL pipette tip. Organoids were disrupted by passage through a 26G needle five times and replated in complete Matrigel. Crypts were counted the next day, and the number of organoids and lobes per organoids were counted on day 6. The percentage of organoids formed was calculated based on the number of enterospheres observed on day 1 after passaging. Crypts were passaged the same way every time, and the medium was changed every third day.

Isolated crypt epithelial cells from the proximal part of mouse small intestine were used for gene expression analysis by qRT-PCR. For ISC and Paneth cell isolation, after crypt isolation, crypts were treated with 30 mL of 4% TrypLE (Invitrogen) for 30–40 min at 37°C, followed by centrifugation at 800 rpm for 5 min. The pellet was resuspended in 15 mL DMEM and centrifuged again at 600 rpm. We discarded the supernatant and sorted Lgr5eGFPhi cells by FACS. For Paneth cell isolation after centrifugation, cells were treated with CD24 antibody, incubated for 30 min on ice, washed with DMEM, and sorted by FACS. RNA was isolated using the QIAGEN RNeasy mini or micro kit. Fifty nanograms of RNA were used per well in a single-step Taqman assay. For quantification of *Wnt1*, *2*, *3*, *3a*, *8a*, *8b*, *10a*, and *10b*, we used primers from Farin et al. (2012). Normalization was done using β Actin, Gapdh, or Hprt. All qRT-PCR data are from RNA isolated from crypts of the proximal part of mouse intestine. Differences were actually more severe in RNA isolated from distal crypts. Because the organoid experiments in this study were performed on the proximal part of the mouse intestine, unless otherwise mentioned, all data generated in this study are from the proximal part of mouse small intestine.

Human Organoid Cultures

Human organoids were grown as described in Mahe et al. (2015). For the medium without Wnt3a, conditioned medium was prepared without adding Wnt3a. Data are from the sixth day after initial plating of human organoids. All experimentation using human tissues described here was approved by an institutional review board (IRB) at CCHMC (IRB #2014-0427) and University of Cincinnati (UC) (IRB #2012-4147). Informed consent for tissue collection, storage, and use of the samples was obtained from the donors at CCHMC or UC. Young refers to 12–16 years of age, and aged refers to 62–72 years of age.

Western Blot

Whole-cell extracts of mouse (proximal intestine) crypt epithelial cells were obtained in radioimmunoprecipitation assay (RIPA) lysis buffer. Nuclear extracts were from mouse (proximal intestine) crypt epithelial cells. Freshly isolated

crypts were lysed for 3 min with cytoplasmic extract (CE) buffer (10 mM HEPES, 60 mM KCl, 1 mM EDTA, 0.075% NP40, 1 mM DTT, and 1 mM PMSF adjusted to pH 7.6. After centrifugation at 1,500 rpm for 5 min, we discarded or stored the CE, and the pellet (nuclei) was washed with CE buffer with NP40, and nuclear extract was prepared from nuclei using standard RIPA lysis buffer. Protein was subjected to standard SDS-PAGE, blotted onto a nitrocellulose membrane/PVDF membrane, and detected using antibodies against Ascl2 (1:1,000 dilution, Millipore, 8F1), β Catenin (1:1,000 dilution, BD Transduction Laboratories), Lamin B (1:500 dilution, Santa Cruz Biotechnology), and Actin (1:1,000 dilution, Sigma).

TUNEL Staining

A TUNEL (in situ cell death detection kit, Roche) assay was used to measure the rate of apoptosis on 6-μm paraffin sections. The number of apoptotic cells per crypt was counted from 15–20 low-power fields (10× magnification).

BrdU Administration and Staining

BrdU (Sigma-Aldrich) was injected at 100 mg/kg body weight, and the intestine was harvested 72 hr after BrdU injection. 6-μm-thick paraffin-embedded tissue sections were deparaffinized, rehydrated, permeabilized by heating in 10 mM sodium citrate buffer, stained with BrdU primary antibody (Santa Cruz, 1:100 dilution in PBS), incubated overnight at 4°C, and incubated with anti-rat FITC-conjugated secondary antibody (Jackson ImmunoResearch Laboratories, 1:200 dilution for 1 hr at room temperature). Pictures were taken under 10× magnification on an Apotome Zeiss microscope. The distance traveled by BrdU was measured using ImageJ software from the crypt base to the midpoint of BrdU-positive cells in a villus.

RNA-Seq and Real-Time PCR on Isolated ISCs and Paneth Cells

RNA from Lgr5eGFPhi-positive cells and Paneth cells sorted by FACS was isolated using QIAGEN RNeasy micro (#74004) following the manufacturer's instructions. Libraries for Lgr5eGFP RNA-seq were prepared using standard Illumina protocols. For Paneth cell transcriptome profiling, the SMARTer Stranded Total RNA-Seq Pico kit from Clontech Laboratories (#635005) was used. The kit generates Illumina-compatible RNA-seq libraries. The cDNA library construction was done as recommended by Clontech, which includes cDNA synthesis, addition of Illumina adapters and barcodes using only limited-cycle PCR, followed by depletion of ribosomal cDNA, further amplification, and purification. The generated libraries were quantitated using an Agilent Technologies bio-analyzer, pooled, and subjected to next-generation sequencing in Hi-Seq 2500 for paired-end 75-bp sequencing conditions. The data were analyzed with Strand NGS (Agilent). Following removal of primers and barcodes, raw reads were aligned to the mm10 mouse genome with annotations provided by University of California Santa Cruz (UCSC). Quantified reads were normalized using the differential expression analysis for sequence count data (DESeq) algorithm. Reasonably expressed transcripts (at least three reads per transcript under more than one experimental condition) were assessed for differential regulation using two-way ANOVAs (p < 0.05) and fold change (FC > 1.5). Ontological enrichments were identified through Database for Annotation, Visualization and Integrated Discover Gene Ontology (DAVID GO). For quantitative real-time PCR of Lgr5GFPhi cells, RNA was amplified, and cDNA was prepared using the NuGEN Ovation RNA amplification system V2 (#3100-12). For quantitative real-time PCR of Paneth cells, RNA amplification and cDNA were prepared using the quantitative real-time PCR SMARTer seq V4 Ultralow input RNA kit for sequencing (#634898).

FAM-Labeled Real-Time PCR Primers for Mouse from ABI
Statistical Analyses

To calculate statistical significance, either Student's t test or Wilcoxon/Mann-Whitney test was used. Error bars indicate SD. GraphPad Prism or Microsoft Excel was used for statistical analysis.

ACCESSION NUMBERS

The accession number for the sequencing data reported in this paper is GEO: GSE84061.

REFERENCES

Barker, N., van Es, J.H., Kuipers, J., Kujala, P., van den Born, M., Cozijnsen, M., Haegebarth, A., Korving, J., Begthel, H., Peters, P.J., and Clevers, H. (2007). Identification of stem cells in small intestine and colon by marker gene Lgr5. Nature 449, 1003–1007.

Barker, N., van de Wetering, M., and Clevers, H. (2008). The intestinal stem cell. Genes Dev. 22, 1856–1864.

Blau, H.M., Cosgrove, B.D., and Ho, A.T. (2015). The central role of muscle stem cells in regenerative failure with aging. Nat. Med. 21, 854–862.

Boj, S.F., Hwang, C.I., Baker, L.A., Chio, I.I., Engle, D.D., Corbo, V., Jager, M., Ponz-Sarvise, M., Tiriac, H., Spector, M.S., et al. (2015). Organoid models of human and mouse ductal pancreatic cancer. Cell 160, 324–338.

Brack, A.S., Conboy, M.J., Roy, S., Lee, M., Kuo, C.J., Keller, C., and Rando, T.A. (2007). Increased Wnt signaling during aging alters muscle stem cell fate and increases fibrosis. Science 317, 807–810.

Farin, H.F., Van Es, J.H., and Clevers, H. (2012). Redundant sources of Wnt regulate intestinal stem cells and promote formation of Paneth cells. Gastroenterology 143, 1518–1529.e7.

Farin, H.F., Jordens, I., Mosa, M.H., Basak, O., Korving, J., Tauriello, D.V., de Punder, K., Angers, S., Peters, P.J., Maurice, M.M., and Clevers, H. (2016). Visualization of a short-range Wnt gradient in the intestinal stem-cell niche. Nature 530, 340–343.

Florian, M.C., Dörr, K., Niebel, A., Daria, D., Schrezenmeier, H., Rojewski, M., Filippi, M.D., Hasenberg, A., Gunzer, M., Scharffetter-Kochanek, K., et al. (2012). Cdc42 activity regulates hematopoietic stem cell aging and rejuvenation. Cell Stem Cell 10, 520–530.

Florian, M.C., Nattamai, K.J., Dörr, K., Marka, G., Uberle, B., Vas, V., Eckl, C., Andrä, I., Schiemann, M., Oostendorp, R.A., et al. (2013). A canonical to noncanonical Wnt signalling switch in haematopoietic stem-cell ageing. Nature 503, 392–396.

Geiger, H., de Haan, G., and Florian, M.C. (2013). The ageing haematopoietic stem cell compartment. Nat. Rev. Immunol. 13, 376–389.

Gregorieff, A., and Clevers, H. (2005). Wnt signaling in the intestinal epithelium: from endoderm to cancer. Genes Dev. 19, 877–890.

Jurk, D., Wilson, C., Passos, J.F., Oakley, F., Correia-Melo, C., Greaves, L., Saretzki, G., Fox, C., Lawless, C., Anderson, R., et al. (2014). Chronic inflammation induces telomere dysfunction and accelerates ageing in mice. Nat. Commun. 2, 4172.

Kamminga, L.M., van Os, R., Ausema, A., Noach, E.J., Weersing, E., Dontje, B., Vellenga, E., and de Haan, G. (2005). Impaired hematopoietic stem cell functioning after serial transplantation and during normal aging. Stem Cells 23, 82–92.

Kim, T.H., Li, F., Ferreiro-Neira, I., Ho, L.L., Luyten, A., Nalapareddy, K., Long, H., Verzi, M., and Shivdasani, R.A. (2014). Broadly permissive intestinal chromatin underlies lateral inhibition and cell plasticity. Nature 506, 511–515.

Koch, U., Lehal, R., and Radtke, F. (2013). Stem cells living with a Notch. Development 140, 689–704.

Kozar, S., Morrissey, E., Nicholson, A.M., van der Heijden, M., Zecchini, H.I., Kemp, R., Tavaré, S., Vermeulen, L., and Winton, D.J. (2013). Continuous clonal tracking reveals small numbers of functional stem cells in intestinal crypts and adenomas. Cell Stem Cell 13, 626–633.

Mahe, M.M., Sundaram, N., Watson, C.L., Shroyer, N.F., and Helmrath, M.A. (2015). Establishment of human epithelial enteroids and colonoids from whole tissue and biopsy. J. Vis. Exp. 97.

Martin, K., Kirkwood, T.B., and Potten, C.S. (1998a). Age changes in stem cells of murine small intestinal crypts. Exp. Cell Res. 241, 316–323.

Martin, K., Potten, C.S., Roberts, S.A., and Kirkwood, T.B. (1998b). Altered stem cell regeneration in irradiated intestinal crypts of senescent mice. J. Cell Sci. 111, 2297–2303.

Metcalfe, C., Kljavin, N.M., Ybarra, R., and de Sauvage, F.J. (2014). Lgr5 stem cells are indispensable for radiation-induced intestinal regeneration. Cell Stem Cell 14, 149–159.

Montgomery, R.K., Carlone, D.L., Richmond, C.A., Farilla, L., Kranendonk, M.E., Henderson, D.E., Baffour-Awuah, N.Y., Ambruzs, D.M., Fogli, L.K., Algra, S., and Breault, D.T. (2011). Mouse telomerase reverse transcriptase (mTert) expression marks slowly cycling intestinal stem cells. Proc. Natl. Acad. Sci. USA 108, 179–184.

Nalapareddy, K., Jiang, H., Guachalla Gutierrez, L.M., and Rudolph, K.L. (2008). Determining the influence of telomere dysfunction and DNA damage on stem and progenitor cell aging: what markers can we use? Exp. Gerontol. 43, 998–1004.

Nalapareddy, K., Choudhury, A.R., Gompf, A., Ju, Z., Ravipati, S., Leucht, T., Lechel, A., and Rudolph, K.L. (2010). CHK2-independent induction of telomere dysfunction checkpoints in stem and progenitor cells. EMBO Rep. 11, 619–625.

Pinto, D., Gregorieff, A., Begthel, H., and Clevers, H. (2003). Canonical Wnt signals are essential for homeostasis of the intestinal epithelium. Genes Dev. 17, 1709–1713.

Potten, C.S., Kovacs, L., and Hamilton, E. (1974). Continuous labelling studies on mouse skin and intestine. Cell Tissue Kinet. 7, 271–283.

Rando, T.A. (2006). Stem cells, ageing and the quest for immortality. Nature 441, 1080–1086.

Reya, T., Duncan, A.W., Ailles, L., Domen, J., Scherer, D.C., Willert, K., Hintz, L., Nusse, R., and Weissman, I.L. (2003). A role for Wnt signalling in self-renewal of haematopoietic stem cells. Nature 423, 409–414.

Rossi, D.J., Jamieson, C.H., and Weissman, I.L. (2008). Stems cells and the pathways to aging and cancer. Cell 132, 681–696.

Sato, T., Vries, R.G., Snippert, H.J., van de Wetering, M., Barker, N., Stange, D.E., van Es, J.H., Abo, A., Kujala, P., Peters, P.J., and Clevers, H. (2009). Single Lgr5 stem cells build crypt-villus structures in vitro without a mesenchymal niche. Nature 459, 262–265.

Sato, T., van Es, J.H., Snippert, H.J., Stange, D.E., Vries, R.G., van den Born, M., Barker, N., Shroyer, N.F., van de Wetering, M., and Clevers, H. (2011). Paneth cells constitute the niche for Lgr5 stem cells in intestinal crypts. Nature 469, 415–418.

Schuijers, J., Junker, J.P., Mokry, M., Hatzis, P., Koo, B.K., Sasselli, V., van der Flier, L.G., Cuppen, E., van Oudenaarden, A., and Clevers, H. (2015). Ascl2 acts as an R-spondin/Wnt-responsive switch to control stemness in intestinal crypts. Cell Stem Cell. *16*, 158–170.

Smith, N.R., Davies, P.S., Silk, A.D., and Wong, M.H. (2012). Epithelial and mesenchymal contribution to the niche: a safeguard for intestinal stem cell homeostasis. Gastroenterology *143*, 1426–1430.

Tian, H., Biehs, B., Chiu, C., Siebel, C.W., Wu, Y., Costa, M., de Sauvage, F.J., and Klein, O.D. (2015). Opposing activities of Notch and Wnt signaling regulate intestinal stem cells and gut homeostasis. Cell Rep. *11*, 33–42.

van der Flier, L.G., Haegebarth, A., Stange, D.E., van de Wetering, M., and Clevers, H. (2009a). OLFM4 is a robust marker for stem cells in human intestine and marks a subset of colorectal cancer cells. Gastroenterology *137*, 15–17.

van der Flier, L.G., van Gijn, M.E., Hatzis, P., Kujala, P., Haegebarth, A., Stange, D.E., Begthel, H., van den Born, M., Guryev, V., Oving, I., et al. (2009b). Transcription factor achaete scute-like 2 controls intestinal stem cell fate. Cell *136*, 903–912.

Wong, V.W., Stange, D.E., Page, M.E., Buczacki, S., Wabik, A., Itami, S., van de Wetering, M., Poulsom, R., Wright, N.A., Trotter, M.W., et al. (2012). Lrig1 controls intestinal stem-cell homeostasis by negative regulation of ErbB signalling. Nat. Cell Biol. *14*, 401–408.

Yamazaki, S., Iwama, A., Takayanagi, S., Morita, Y., Eto, K., Ema, H., and Nakauchi, H. (2006). Cytokine signals modulated via lipid rafts mimic niche signals and induce hibernation in hematopoietic stem cells. EMBO J. *25*, 3515–3523.